RSC Advances

This is an *Accepted Manuscript*, which has been through the Royal Society of Chemistry peer review process and has been accepted for publication.

Accepted Manuscripts are published online shortly after acceptance, before technical editing, formatting and proof reading. Using this free service, authors can make their results available to the community, in citable form, before we publish the edited article. This *Accepted Manuscript* will be replaced by the edited, formatted and paginated article as soon as this is available.

You can find more information about *Accepted Manuscripts* in the Information for Authors.

Please note that technical editing may introduce minor changes to the text and/or graphics, which may alter content. The journal's standard Terms & Conditions and the Ethical guidelines still apply. In no event shall the Royal Society of Chemistry be held responsible for any errors or omissions in this *Accepted Manuscript* or any consequences arising from the use of any information it contains.

ROYAL SOCIETY OF CHEMISTRY

www.rsc.org/advances

1-D/2-D Hybrid Nanostructured Manganese Cobaltite-Graphene Nanocomposite for Electrochemical Energy Storage

A. Nirmalesh Naveen[a,*], Subramanian Selladurai[a]

[a] Ionics lab, Department of Physics, Anna University, Chennai, Tamil Nadu, India 600025

Corresponding author – A. Nirmalesh Naveen

Phone no- +91 9962239031

Postal Address - Ionics Lab.,
Department of physics,
Anna University,
Chennai, Tamil Nadu,
India. 600025

RSC Advances Accepted Manuscript

ABSTRACT

Unique 1-D/2-D hybrid nanostructured manganese cobaltite-graphene nanocomposite (GMC) was synthesized by facile hydrothermal method. Successful composite formation was determined from structural study like XRD and chemical analyses like FTIR and XPS. FESEM and TEM observations of the manganese cobaltite compound reveal the flower like architecture formed by the clusters of $MnCo_2O_{4.5}$ nanowires. By graphene incorporation a unique hybrid 1-D/2-D nanostructure was developed in the composite material. BET surface area measurement reveals the extremely high surface area of the composite material owing to its distinct morphology. CV measurements reveal the excellent redox reactivity of the prepared electrode materials. GMC

exhibited a high specific capacitance of 890 F/g which upon activation over cycling increases to 934 F/g. $MnCo_2O_{4.5}$ decorated graphene sheets in the composite provides high interfacial sites for the redox process, exceptional electrical support and mechanical strength during cycling. The manganese cobaltite-graphene composite was able to retain 95% of its original capacitance at the end of 2000 cycles. The small solution resistance value of 1.21 Ω illustrates the superior conductivity of the composite material. A symmetrical cell fabricated using GMC electrode material exhibited a maximum specific capacitance of 189 F/g at 5 mV/s scan rate. Fast reaction kinetics displayed by the cell was due to the charge transfer speedway provided by the graphene sheets. Superior performance of the hybrid composite makes it a potential candidate for supercapacitor applications.

KEYWORDS: Nanowires, Hybrid nanostructure, Graphene nanocomposite, Supercapacitor, Faradaic behaviour.

1. Introduction

Besides the energy crisis, serious environmental concerns about CO_2 emission from fossil fuels have forced to search for alternative, efficient and non-pollutant ways of energy generation, transportation and storage [1-5]. Electrochemical capacitors or supercapacitors are gaining much interest as an energy storage device owing to their small size, flexibility, high power characteristics, stability and long cycle life. They are superior to conventional capacitors and batteries in terms of energy density and power density respectively. These unique features made them desirable for many applications such as hybrid vehicles, tapping transient energy from renewable energy resources, engine ignition and power backups [6-7]. Relatively, low gravimetric energy density limits supercapacitor from augmenting batteries. Carbonaceous

RSC Advances Accepted Manuscript

materials store electrical energy by forming electric double layer at the electrode/electrolyte interface. Charge stored is very small due to poor utilization of the electrode material i.e. only surface species participate in the reaction. Whereas, in transition metal oxides and conducting polymers charge storage takes place by charge transfer at the surface and within the bulk of the material by faradaic redox process. Hence, the specific capacitance exhibited by these materials is substantially higher compared to electric double layer capacitance [8-11]. Remarkable capacitive performance exhibited by hydrous ruthenium oxide ($RuO_2.H_2O$) and iridium oxide (IrO_2) has opened up possibility for other transition metal oxides to be used as an electrode material [12].

Mixed transition metal oxides, typically ternary metal oxides with two different metal cations, have received an upsurge of interest in recent years due to their promising roles in many energy-related applications. Spinel cobaltites are a class of materials with molecular formula MCo_2O_4 (M- Ni, Mn, Zn, Cu) that are attractive for their superior performance in wide areas of applications [13]. For supercapacitors, $NiCo_2O_4$ is most studied for its high electrical conductivity and rich redox chemistry compared to individual cobalt oxide and nickel oxide [14]. The coupling of two metal species could make oxidation-state-rich redox reactions which are essential for pseudocapacitor and various combinations of the cations during the charging-discharging process, and the tunable stoichiometric/non-stoichiometric compositions of the mixed transition metal oxides could provide great opportunities to manipulate the physical/chemical properties [15]. $MnCo_2O_4$ is an important member of the mixed valence oxides with spinel structure, which showed excellent electrochemical activity in alkaline solutions due to the redox-active metal centers. In manganese cobalt oxide, cobalt shows a higher oxidation potential while manganese can transport more electrons and bring in higher capacity

RSC Advances Accepted Manuscript

[16]. $MnCo_2O_4$ was extensively studied as an electrode material for lithium ion batteries but one can find only hand full of literatures on $MnCo_2O_4$ for supercapacitor applications. Investigations on manganese cobaltite, an important representative of Co-based oxide was restricted because of the close relationship between microstructure and electrochemical performance. One-dimension nanowire arrays have attracted intense attention for their excellent physical and chemical properties and are promising electrode materials for supercapacitors [17-19]. The nanowire array architecture, just as the sphere-like particle, is one of the architectures which can provide large specific area, resulting in high utilization of active materials. In spite of some attractive features such as low price, relatively high electrical conductivity and stability, $MnCo_2O_4$ suffers from poor ionic conductivity and partial dissolution in alkaline electrolytes leading to decay in capacitance. Despite some disappointing features, $MnCo_2O_4$ can be exploited through some modification or combination with carbonaceous materials, which are light weight and possess high electronic conductivity [20].

Graphene is a two dimensional arrangement of one atom thick sp^2 carbon atoms. Compared with other carbon materials, graphene is a more attractive supporting material due to its high surface area, fast two-dimensional electron-transfer kinetics, and high stability. Owing to these properties graphene is preferred as a platform for decoration of metal oxides to avoid their agglomeration hence increased utilization of nanoparticles [21-23]. Graphene is also known for its exceptional electrical conductivity and mechanical strength. By decorating $MnCo_2O_4$ nanoparticle over graphene sheets, agglomeration of the particles can be avoided at the same time stacking of graphene sheets is also prevented; graphene template provides excellent electrical and electronic conductivity to the metal nanoparticles during charge storage, and by graphene encapsulation Mn ion dissolution in alkaline electrolytes can be seized, resulting in an

RSC Advances Accepted Manuscript

enhanced cycling stability. Hence, graphene addition to $MnCo_2O_4$ will circumvent all the shortcomings that limit its application for supercapacitors. Previously, Li et al and Yuan et al have demonstrated that by simple addition of carbonaceous material, the specific capacitance, conductivity, rate kinetics and charge retention ability have increased tremendously [6, 20]. However, their methods were either exhaustive or includes toxic surfactants which are not desirable for commercial production. Hence, here we have deduced a simple environmental benign industry scalable method for the synthesis of $MnCo_2O_{4.5}$-graphene composite.

In this present work, for the first time, we have prepared and studied $MnCo_2O_{4.5}$ nanowire-graphene composite for supercapacitor applications. Composite prepared was subjected to various physio-chemical characterizations to understand its respective properties. Electrochemical characterizations revealed the superior performance of the synthesized electrode material.

2. Experimental section

2.1 Materials

All the chemicals used for synthesis process were analytical grade. Microcrystalline graphite powder, potassium permanganate ($KMnO_4$), sulfuric acid (H_2SO_4), orthophosphoric acid (H_3PO_4), hydrogen peroxide (H_2O_2), cobaltous acetate, manganese acetate and urea were used as purchased without further purification.

2.2 Graphene oxide (GO) preparation

Graphene oxide was prepared using graphite as the starting material by slight modification in the improved Hummer's method. Briefly, 1.6 g of graphite powder was added to

RSC Advances Accepted Manuscript

the mixture of 160 mL H_2SO_4 and 40 mL orthophosphoric acid (4: 1 ratio) under stirring. To the vigorously agitated solution, 9 g of $KMnO_4$ (oxidant) was added in small portions with 10 minutes time interval at ambient conditions. The mixture was left for 3 days under stirring at room temperature for complete oxidation of graphite. To the mixture H_2O_2 was added which reacts exothermically turning the dark reactant solution into brilliant yellow colour indicating the complete oxidation of graphite oxide. Yellow coloured solution containing GO precipitate was washed by pouring HCl solution into it under stirring and the precipitate was allowed to settle down under the action of gravity. After 24 h the resultant clear solution at the top was decanted slowly and the above procedure was repeated. Washing with HCl solution was necessary to remove the sulfate ions from the product. Similar procedure was followed for washing with deionized water until pH=7 were arrived. Final precipitate was collected by centrifuging at high rpm. The brown precipitate collected was dried at 60 ˚C for 24 h and stored. GO was exfoliated by taking a small amount of GO in a closed crucible and heating it at 150 ˚C in muffle furnace at air atmosphere prior to the composite formation.

2.3 Manganese cobaltite – reduced graphene oxide (RGO) composite preparation

In this typical synthesis procedure, stoichiometric proportions of manganese acetate (0.01 M) and cobaltous acetate (0.02 M) were added to a 200 ml mixed solution of water and ethanol (9:1). The mixture solution was stirred vigorously for 30 min to obtain homogenous solution. To this, 100 mg of Ex-GO (exfoliated GO) was added and stirred 0.5 h more. Later, excess amount of urea (0.05 M) was added to this reaction mixture. After 15 min of stirring the solution was transferred to a reaction vessel and placed at 120 ˚C for 6 h. The black precipitate obtained was collected and washed repeatedly using de-ionized water and ethanol. As obtained powder was

RSC Advances Accepted Manuscript

calcined at 400 ˚C for 2 h at the heating rate of 1˚/min and labeled as GMC. Bare manganese cobaltite was prepared by the same procedure excluding GO and labeled as MC.

2.4 Physio-chemical characterization of the samples

X-ray diffractogram of the samples were recorded by Bruker X-ray diffractometer model D2 PHASER. Kα radiation of copper target with a wavelength of 1.5416 Å was used as X-ray source. Detected diffraction angle (2θ) was scanned from 10^o to 80^o with a step size of 0.02^o. FTIR spectra of the samples were recorded between 400 cm^{-1}- 4000 cm^{-1} wave number using FTIR spectrophotometer (Bruker). Morphology of the prepared samples was imaged using FEI Quanta FEG 200 – Field Emission Scanning Electron Microscope (FESEM). High Resolution Transmission Electron Microscope images were recorded for the samples using Jeol JEM 3010 electron microscope. X-ray photoelectron spectra (XPS) were recorded using Kratos AXIS Ultra DLD X-ray photoelectron spectrometer with aluminium anode (monochromatic Kα X-rays of energy 1.486 eV) as source and operating at 160 eV pass energy. All binding energy values were charge-corrected to the C 1s signal which was set at 284.6 eV. XPS spectra were analyzed and fitted using Casa XPS software (version 2.3.16).

2.5 Fabrication of electrode and electrochemical performance test

Prepared electrode material, activated carbon and polyvinylidene fluoride (PVDF) binder were mixed together in the ratio of 85:5:10 (wt. %). A slurry of the mixture was made using N-Methyl-2-Pyrrolidone (NMP), which was coated onto a nickel foil current collector of (1 x 1 cm) 0.25 mm thickness (produced by Alfa Aesar) and dried for 4 h to remove the solvent. The mass of the loaded samples lies within the range of 0.4 - 0.5 mg measured using a Shimadzu analytical balance of accuracy 0.01 mg. Cyclic Voltammetry (CV), Chronopotentiometry (CP) and Electrochemical Impedance Spectroscopy (EIS) were performed using a CHI 661C

RSC Advances Accepted Manuscript

electrochemical workstation employing a standard 3-electrode cell configuration with platinum wire as counter electrode and Standard Calomel Electrode (SCE) as a reference electrode. The measurements were performed using aqueous 3 M KOH electrolyte at ambient conditions within 0 – 0.65 V potential windows. A detailed procedure on symmetric assembling of electrode in a 2 electrode configuration is provided in the supplementary information.

3. RESULTS AND DISCUSSION

3.1 XRD studies

X-ray diffraction technique was employed to investigate the crystallinity and phase formation of the prepared samples. Figure 1 presents the diffraction pattern recorded for MC and GMC. Inset of the figure shows the diffraction spectrum of GO. The peak at $2\theta = 10.04^{\circ}$ and 42.3° corresponds to the (001) and (100) reflections of GO respectively [24]. Pristine graphite generally exhibit a peak at $2\theta = 26.3^{\circ}$ attributed to its (002) plane with a lattice spacing of 0.34 nm. Due to the introduction of various oxygen containing functional groups namely, hydroxyl, epoxy and carboxyl groups attached to the basal planes and edges of the crystal plane, lattice spacing increases to 0.87 nm and the peak shifts towards the lower angle region of the spectrum [25]. Thermal analysis reveals that the phase formation of the samples occurred at temperatures less than 400 ˚C (Figure S1 of electronic supplementary information (ESI)).

RSC Advances Accepted Manuscript

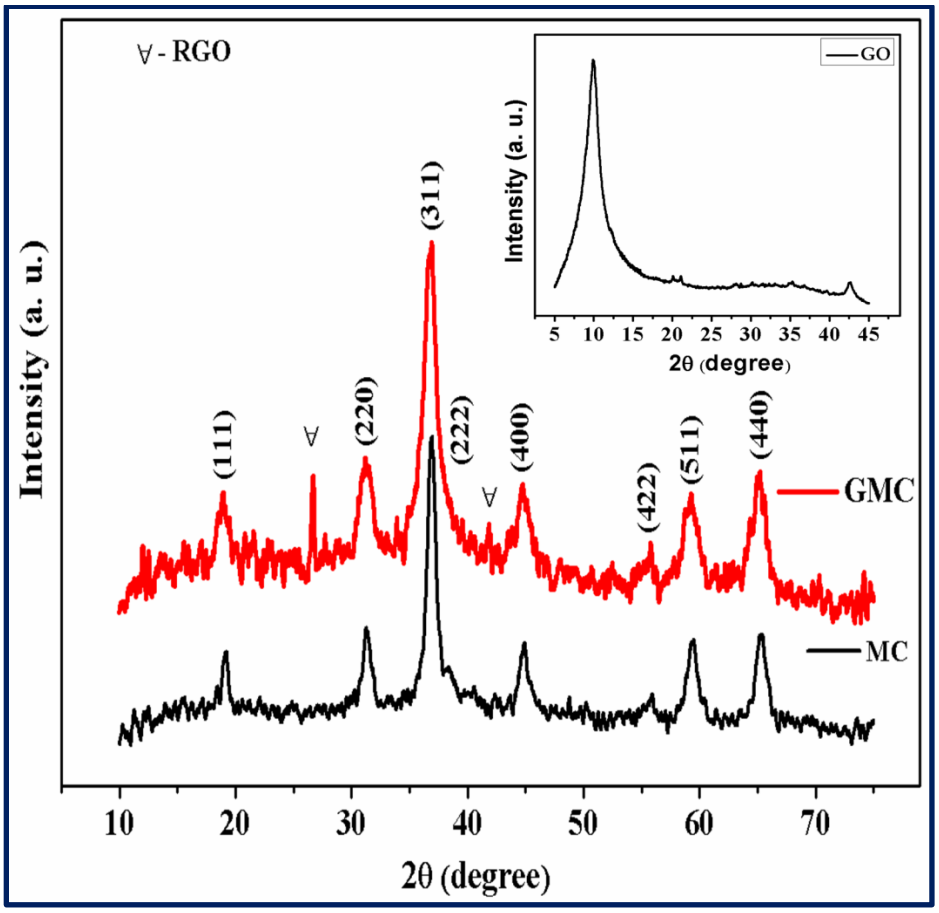

Figure 1. Shows the X-ray diffraction pattern (XRD) recorded for the samples MC and GMC. Inset of the figure shows the XRD pattern of GO.

Eight prominent diffraction peaks were observed for both MC and GMC composite. Peaks can be indexed to (111), (220), (311), (222), (400), (422), (511) and (440) planes of cubic manganese cobaltite ($MnCo_2O_{4.5}$) with space group fd3m (JCPDS card no. 032-0297) [26]. Lattice constant of $MnCo_2O_{4.5}$ is generally found to be lower than that of $MnCo_2O_4$. In our case cell parameter of MC was determined experimentally as 8.07 Å. Apart from the peaks corresponding to $MnCo_2O_{4.5}$, GMC also contains characteristic peaks of RGO at $2\theta = 26.7^{\circ}$ and 41.85°. Reappearance of peak at $2\theta = 26.70^{\circ}$ and decrease in lattice spacing to 0.37 nm indicates the successful reduction of RGO. Removal of oxygen containing functional groups from GO has

RSC Advances Accepted Manuscript

resulted in contraction of lattice spacing and re-establishment of conjugated sp^2 carbon network. This confirms the successful formation of the $MnCo_2O_{4.5}$-RGO composite. With graphene introduction cell parameter of GMC increases to 8.09 Å and a slight peak shift towards left hand side of the spectrum was noticed. Decrease in crystallinity of the composite material can be observed from the XRD pattern. Introduction of graphene have introduced more structural defects which can provide more diffusion channels for electrolyte ions to improve the electrochemical activity [1]. Generally, amorphous nature favors higher ionic conductivity than crystalline or highly ordered structure in materials. Decrease in the crystallite size of the GMC sample was noticed from the peak broadening. Average crystallite size were calculated for the samples using Scherrer formula given below

$$d = \frac{0.9\times \lambda}{\beta \cos\theta} \quad (1)$$

d is the crystallite size, λ is the X-ray wavelength (1.542 Å), θ is the Bragg diffraction angle and β is the full width at the half maximum (FWHM) of the diffraction peak [27]. Crystallite size of 10 nm calculated for MC decreases to 7 nm in the composite. This observation once again suggests that graphene introduction reduces the agglomeration of the particles.

3.2 FTIR Analysis

FTIR spectra recorded between 400 cm^{-1} to 4000 cm^{-1} for the prepared samples is shown in figure 2. As shown in Fig. 2 (a), GO spectrum reveals the presence of various oxygen containing functional groups attached to the graphite lattice. Band at 3411 cm^{-1} and 1628 cm^{-1} was attributed to the stretching vibrations and deformation vibrations of hydroxyl groups respectively [28].

RSC Advances Accepted Manuscript

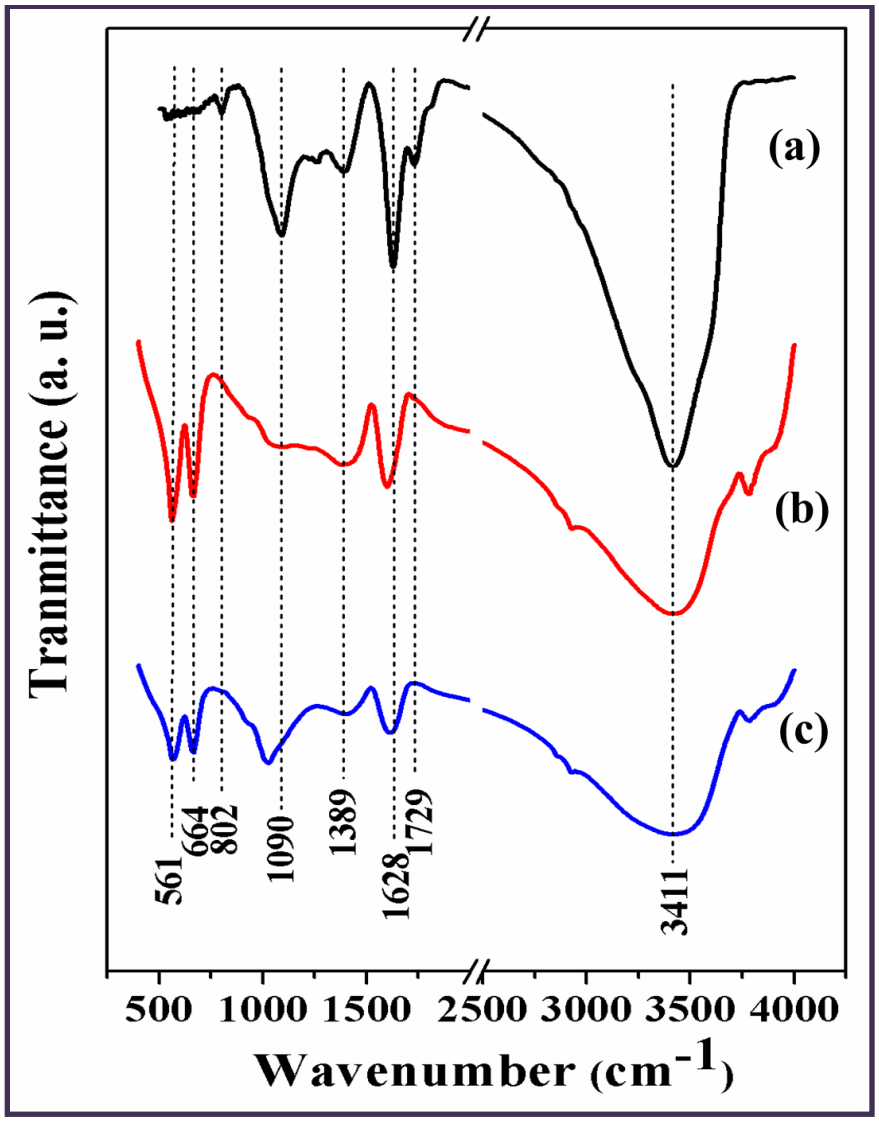

Figure 2. Presents the FTIR spectra acquired between 400 to 4000 cm^{-1} for (a) GO, (b) MC and (c) GMC.

The stretching vibrations of epoxy (C-O) were observed at 1090 cm^{-1}. The peak at 802 cm^{-1} is attributed to the asymmetric stretching of CO [29]. Appearance of a peak at 1389 cm^{-1} was may be due to the presence of tertiary C–OH groups. C=O stretching vibration of sp^2 carbon belonging to carboxyl COOH groups situated at the edges of graphite oxide sheets was located at 1729 cm^{-1} [30]. FTIR spectrum of MC and GMC is displayed in Fig. 2 (b) and (c) respectively. A pair of peaks appeared in the low wavenumber region of the spectra is typical of spinel type

RSC Advances Accepted Manuscript

compounds. Observed peaks were characteristics of metal oxygen stretching vibrations, peak at 561 cm^{-1} corresponds to that of metal ion residing at the octahedral site and peak at 664 cm^{-1} corresponds to the metal ion at tetrahedral site in the spinel compound. Two different positions of metal–oxygen bands are due to the difference in bond length between the metal cations and oxygen anions present on tetrahedral and octahedral sites [31]. Peaks corresponding to various oxygen containing functional groups observed in the case of GO either disappeared or were suppressed in the FTIR spectrum of GMC. This observation confirms the successful reduction of RGO and composite formation. Band around 3426 cm^{-1} and 1608 cm^{-1} can be attributed to the OH stretching vibrations present in the structurally bonded water and those bonded to the metal ions respectively.

3.3 Morphology analysis

FESEM images were taken to investigate the surface morphology of the samples. Figure 3 (a) and (b) shows the low and high magnification images of flower like $MnCo_2O_{4.5}$ nanowire arrangements. Flower like structure of the $MnCo_2O_{4.5}$ is clearly composed of several thin nanowires. High magnification image reveals the tentacles like thin nanowires protruding from the center of the flower structure.

RSC Advances Accepted Manuscript

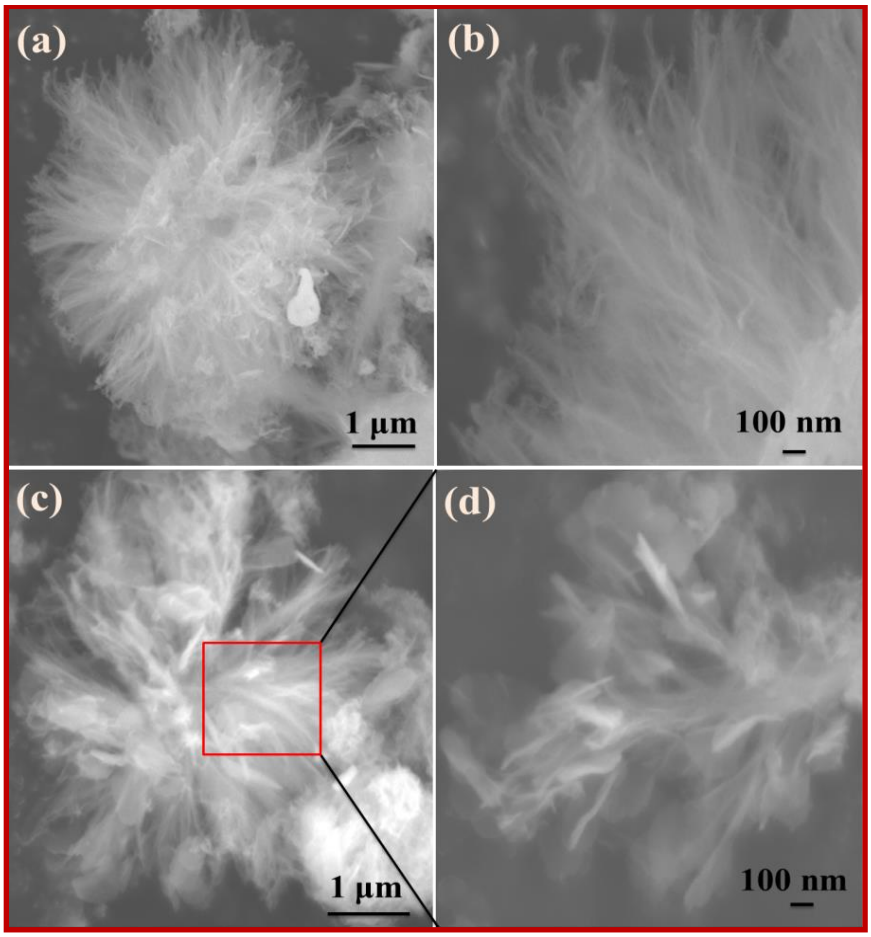

Figure 3. Displays the FESEM images captured at low and high magnifications of MC (a-b) and GMC (c-d) samples.

Figure 3 (c) and (d) shows the low and high magnification images of GMC sample. Nano-flower like morphology with nanowire tentacles was retained in the graphene-manganese cobaltite composite. Additionally, it can be observed that graphene sheets are clinging to the nanowires of $MnCo_2O_{4.5}$. High magnification image clearly reveals the leaf like graphene sheet attached to the protruding branches of nanowire. Uniform distribution of graphene sheets throughout the flower architecture suggest the intrinsic electrical contact between the individual sheets and the nanowires rather merely placed on them. Pre-exfoliation of GO has increased the interfacial contact area between manganese cobaltite nanoparticles and graphene sheets during composite

RSC Advances Accepted Manuscript

formation and provided the opportunity for an individual graphene sheets to attach to an individual nanowires. Figure S2 of the ESI provides the FESEM images captured for as obtained MC and GMC before calcination and graphene sheets obtained without $MnCo_2O_{4.5}$ nanowires.

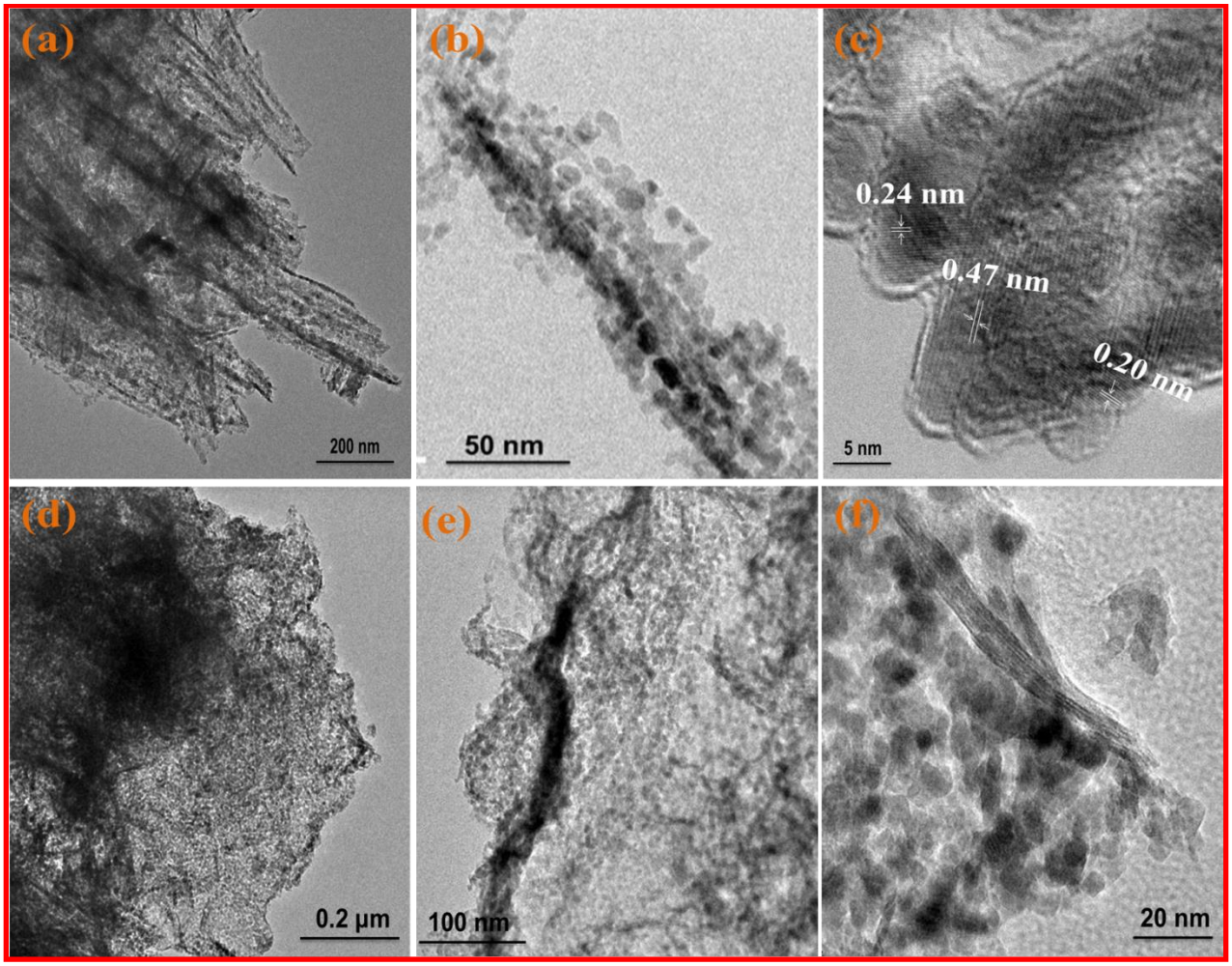

Figure 4. (a) and (b) shows the TEM images of cluster of $MnCo_2O_{4.5}$ nanowires and individual nanowire in MC respectively, (c) HRTEM image depicts the polycrystalline nature of the nanowires, (d) and (e) shows the low and high magnification images of manganese cobaltite nanoparticles decorated over graphene sheets in GMC and (e) exhibits the mesoporous nature of the particles.

RSC Advances Accepted Manuscript

This typical synthesis method has provided the possibility to incorporate the advantages of 1-D and 2-D nanostructure. Graphene sheets in the composite can increases the electrode-electrolyte interfacial area advantageous for facile redox process, while $MnCo_2O_{4.5}$ conducting nanowires can play a dual role both as participant and electron transport cables. Such hybrid nanostructures are most desirable for ultrafast and highly efficient charge storage. EDAX spectra recorded for the samples were provided in Fig. S3 of ESI. Detailed investigation on the surface morphology of the samples was carried out using HRTEM images. Figure 4 (a-c) and (d-f) displays the HRTEM images of MC and GMC respectively. Nanowire structure of MC was confirmed from the low magnification TEM image, as shown in Fig.4 (a). Clearly, each nanowire was composed of numerous $MnCo_2O_{4.5}$ crystallites. Fig. 4 (b) shows the TEM image of individual nanowire with diameter ~57 nm and length extending to few hundreds of nanometer. Growth of one dimensional nanoparticle without the use of toxic growth directing agents or surfactants is an important credit to this typical synthesis method. HRTEM images reveal the polycrystalline nature of the prepared nanowires, seen in Fig 4 (c).

The interlayer distance of randomly selected nanoparticle was calculated to be 0.47 nm, 0.24 nm and 0.20 nm, which agrees well with the (111), (311) and (400) lattice planes. The d spacing values calculated from the HRTEM images were coherent with those calculated from the XRD measurements. Figure 4 (d) and (e) depicts the nearly monodispersed mesoporous nanoparticles decoration over the graphene sheet which was transparent under the electron beam due to its excellent conductivity. From fig. 4 (f) size of the particles were calculated, which lies between 6-8 nm. This confirms the reduction in particle size and the results are in good agreement with the XRD studies.

RSC Advances Accepted Manuscript

3.4 Surface Area Analysis

The material was characterized further by obtaining nitrogen adsorption and desorption isotherms to investigate the BET surface area and porous structure (figure 5). The isotherms of MC and GMC can be categorized as type IV according to the IUPAC classification with a distinct hysteresis loop, indicating the presence of a mesoporous structure [32]. Remarkably, high BET surface area of 99.25 m^2/g was observed for MC which can be attributed to the flower like structure made up of one dimensional nanowires observed from the imaging techniques. When, 2-D graphene was added to the 1-D nanowires of manganese cobaltite, the specific surface area increased abruptly to 150.55 m^2/g. In spite of the same morphology as bare manganese cobaltite the high surface area of graphene-manganese cobaltite composite material can only be attributed to the incorporation of graphene sheets. To justify this attribution, N_2 adsorption and desorption measurements was conducted for graphene sheets and the results are provided in Figure S4 of the ESI. BET calculations for bare graphene sheets reveal a high surface area of 245 m^2/g. Such, hybrid nanostructures could offer exceptional interfacial area to facilitate rapid electrochemical reactions. Obtained surface area is higher than previously reported structures like nanoflakes [33], hierarchical architectures [34], microspheres [13], hollow submicrospheres [35] and nanowires [16]. According to the Barrett–Joyner–Halenda (BJH) pore size distribution data (provided alongside of their respective isotherms), the average pore size of MC and GMC was estimated as 27.19 nm and 20.84 nm respectively, confirming the mesoporous nature. From the distribution curve of GMC, predominant number of pores size ranges between 2-5 nm. It is well established that the pore size of the electrode within 2-5 nm is optimal for the behavior of supercapacitors, which is beneficial to the transport and diffusion of ions since the nanoscale pores can facilitate penetration of the electrolyte and ions through bulky electrodes [2].

RSC Advances Accepted Manuscript

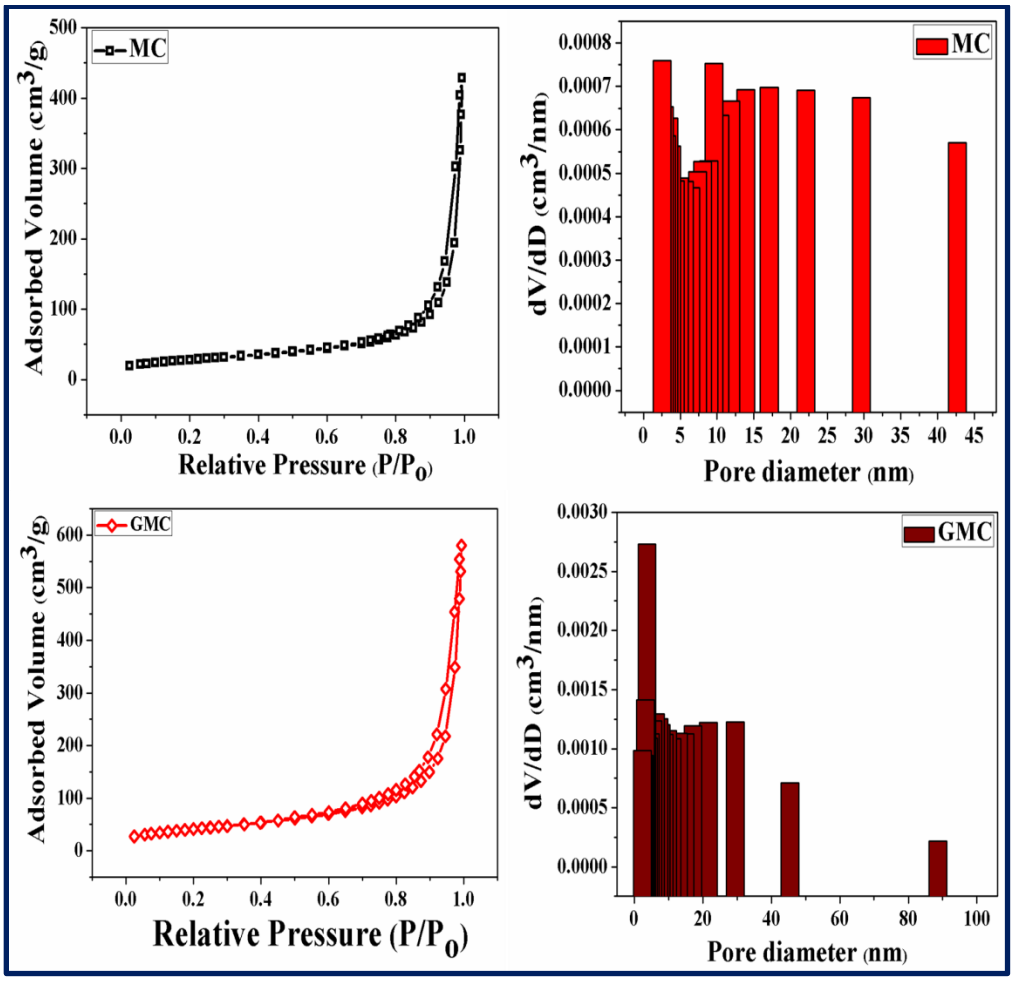

Figure 5. Shows the N_2 adsorption-desorption isotherms recorded for the samples MC and GMC with their respective pore size distribution on the right side.

Pore volume another important parameter of the electrode material was also obtained from the BJH method. Pore volume of 0.66 cm^3/g measured for MC increases to 0.90 cm^3/g for GMC sample. GMC has exhibited mesoporous nature, high surface area and pore volume, hence we speculate that the hybrid structured composite could demonstrate enhanced electrochemical performances than MC as supercapacitor electrode material.

RSC Advances Accepted Manuscript

3.5 X-ray Photoelectron Spectroscopy studies (XPS)

XPS measurements were conducted to make qualitative and quantitative chemical analysis of the prepared samples. Results of the XPS analysis were provided in figure 6. Survey spectrum recorded for MC and GMC is provided in Fig. 6 (a).

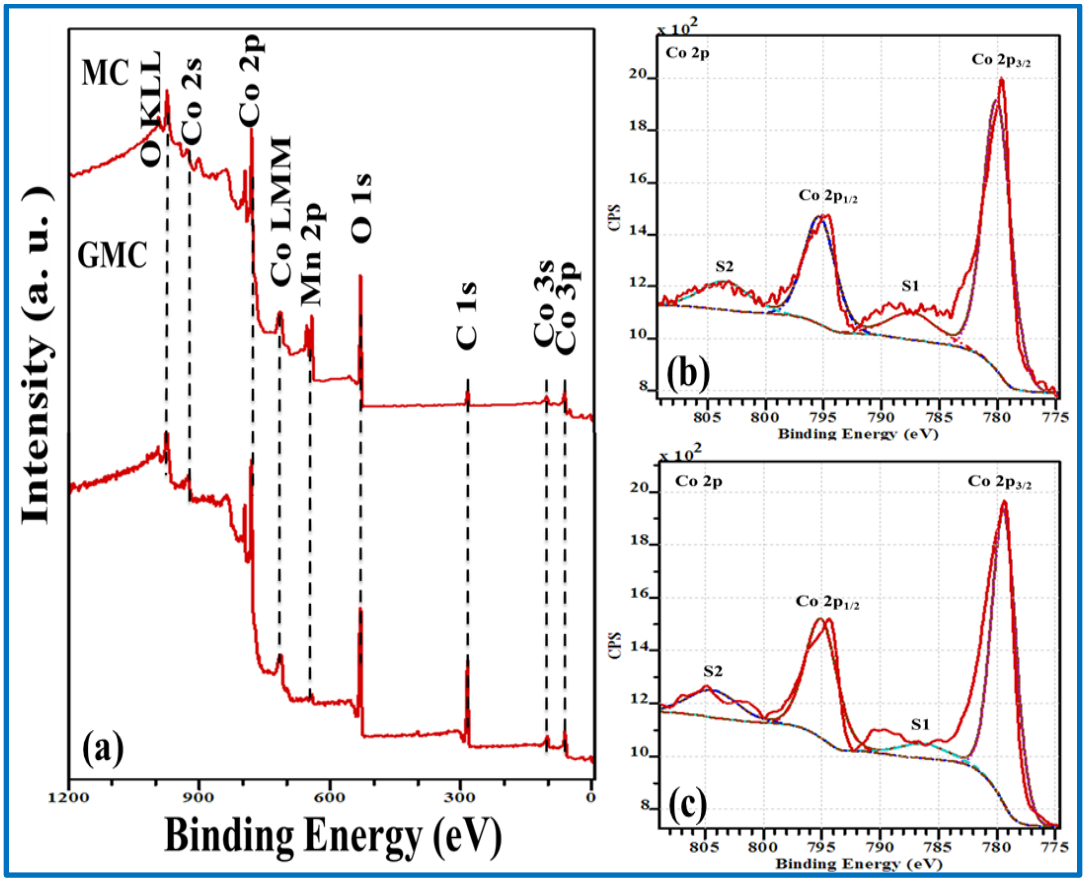

Figure 6. Presents the XPS results, (a) the survey spectrum of MC and GMC, (b) and (c) Co 2p spectrum of MC and GMC respectively

Elements corresponding to $MnCo_2O_{4.5}$ were observed along with carbon. Absence of elements other than those present in the molecular formula indicates the chemical purity of the prepared samples. In GMC, the carbon content is higher than MC suggesting the incorporation of graphene in the composite. To acquire details about oxidation state of cobalt and manganese

RSC Advances Accepted Manuscript

ions, Co 2p and Mn 2p high resolution spectrum were deconvoluted. Figure 6 (b) and (c) presents the deconvoltued high resolution Co 2p spectrum of MC and GMC respectively. Spin orbit doublets of Co 2p was observed at a binding energy of 779.37 eV (Co $2p_{3/2}$) and 795.03 eV (Co $2p_{1/2}$) for MC. Additionally two shake up satellites were observed at 786.29 eV and 804.34 eV. Orbital splitting energy of 15.66 eV and appearance of satellite peak are typical of a spinel cobaltite.

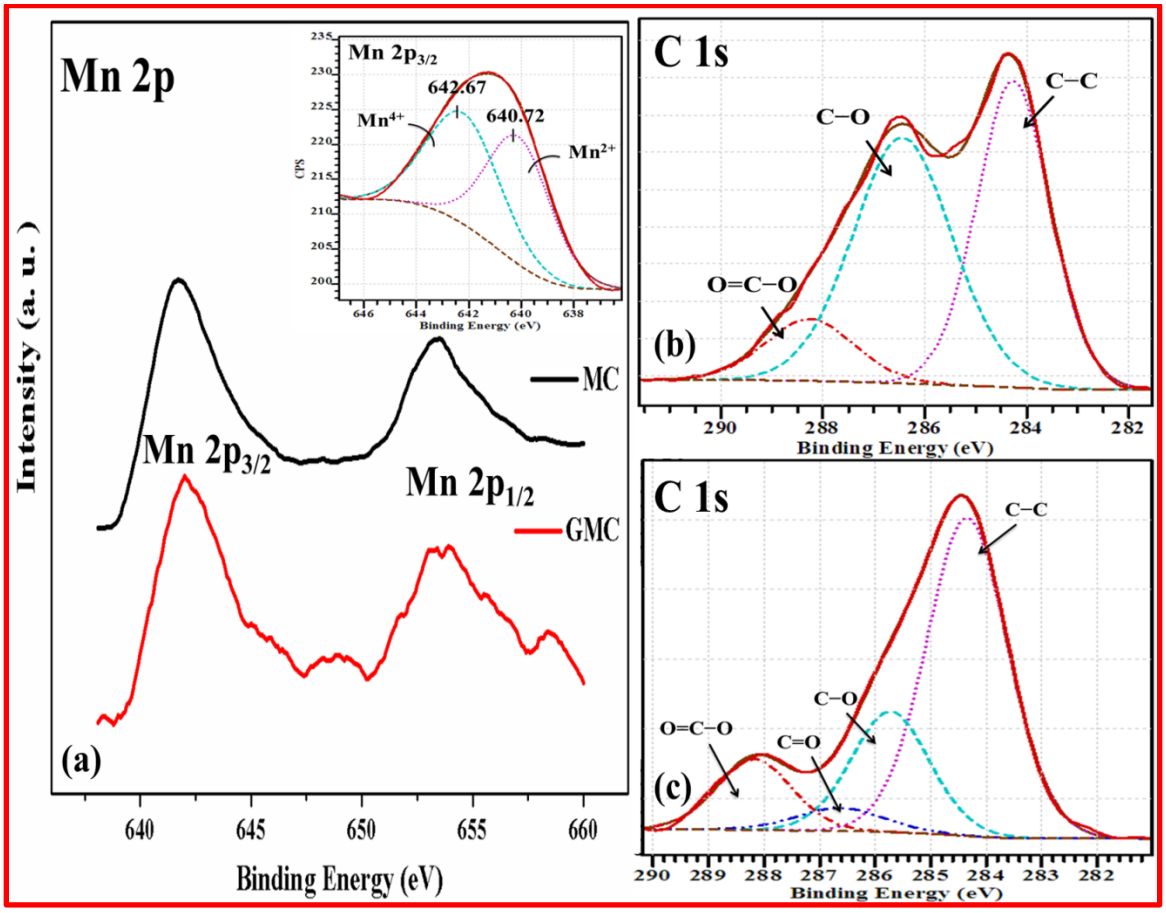

Figure 7. (a) Displays the Mn 2p spectra obtained for MC and GMC and inset of the figure contains the deconvoluted Mn $2p_{3/2}$ spectrum of MC, the high resolution deconvoluted C 1s spectrum of GO and GMC composite is shown in (b) and (c) respectively.

RSC Advances Accepted Manuscript

Appearance of first satellite peak at 3.5 – 6.5 eV above the Co $2p_{3/2}$ peak is characteristic of Co^{2+} ions, and second satellite peak at 9 – 10 eV above the Co $2p_{1/2}$ main peak is characteristic of Co^{3+} ions [36]. Co 2p of GMC also contains similar features with negligible changes in the binding energies. Mn 2p high resolution spectrum of MC and GMC is provided in Fig. 7 (a). Peaks at 641.67 eV and 653.36 eV correspond to Mn $2p_{3/2}$ and Mn $2p_{1/2}$ spin orbit doublets of Mn 2p with spin orbital splitting energy of 11.69 eV. Peak appearing at 641.67 eV suggest the presence of two types of Mn ions. Inset of the figure consist of the deconvoluted Mn $2p_{3/2}$ peak. Component peaks at 640.72 eV and 642.67 eV are attributed to Mn^{2+} and Mn^{4+} ions present in the compound. Obtained results are in good agreement with previous reports [37]. Figure 7 (b), displays the C 1s spectrum of GO demonstrating the presence of various oxygen containing functional groups. C 1s spectrum of GMC is provided in Fig. 7(c) which illustrates the successful removal of carboxylic, epoxy and hydroxyl group in the composite [38]. To summarize, two types of cobalt and manganese ions were determined to be present in the compound and GO reduction was confirmed from the XPS results.

3.6 Electrochemical Characterizations

3.6.1 Cyclic voltammetry

Electrochemical characteristics of the sample were examined using cyclic voltammetry technique in a three electrode cell configuration. Figure 8 shows the CV curve recorded at 25 mV/s scan rate in 3 M KOH electrolyte for the prepared electrode materials. Appearance of redox peaks in the CV curve and deviation from rectangular shape suggest the typical faradaic redox behaviour of the electrode materials [39]. CV curve of MC was composed of two anodic peaks centering at 0.39 V and 0.45 V and a cathodic peak at 0.31 V. In the case of GMC, a pair of redox peaks was observed at 0.49 V (anodic) and 0.38 V (cathodic). Pair of anodic peaks

RSC Advances Accepted Manuscript

observed for MC has merged together to form a single composite peak, which may be due to the rapid charge transfer provided by graphene in the composite. It is to be expected for a binary solid state redox couple $Mn^{3+/}Mn^{2+}$ and $Co^{3+/}Co^{2+}$ in the $MnCo_2O_4$ structure that provides plenty of electroactive sites to undergo facile redox process. Redox peaks in the CV curve originates from the reversible transitions between the oxidation states of Mn/Co ions. Since, manganese and cobalt ions undergo oxidation and reduction at similar potentials, it is difficult to distinguish between peaks corresponding to manganese and cobalt ions in the CV curve distinctly. The large value of current density in the voltammogram can be associated with the faradaic transition of manganese ions ($Mn^{2+}\leftrightarrow Mn^{3+}$) and cobalt ions ($Co^{2+}\leftrightarrow Co^{3+}$ and $Co^{3+}\leftrightarrow Co^{4+}$).

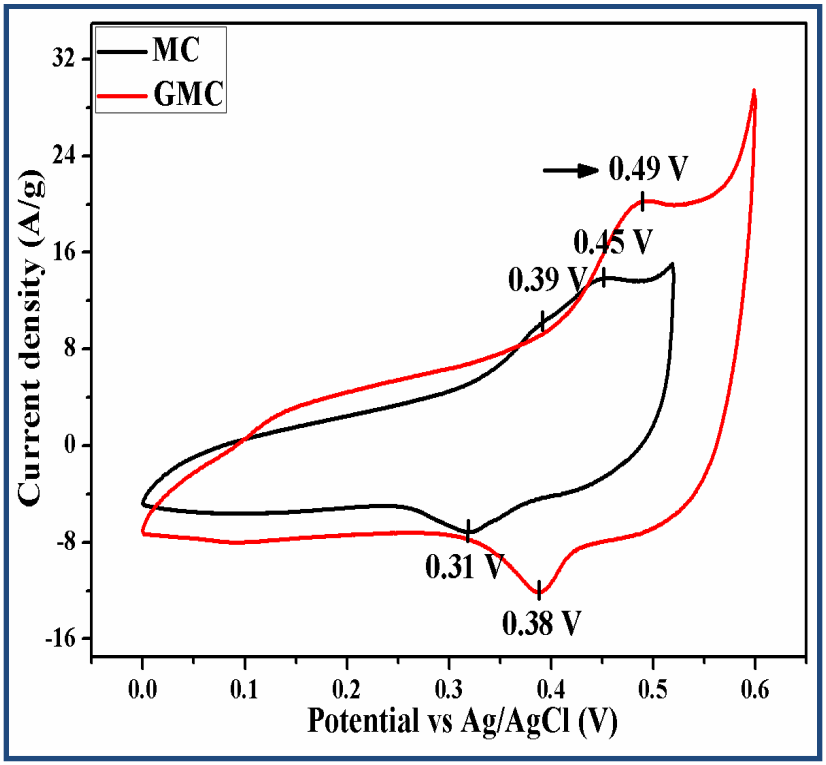

Figure 8. Exhibits the CV curves of MC and GMC recorded at 25 mV/s scan rate in 3 M KOH aqueous electrolyte.

The electrochemical reaction of $MnCo_2O_4$ with the electrolyte can be written as follows [40]

RSC Advances Accepted Manuscript

$$MnCo_2O_4 + H_2O + OH^- \leftrightarrow 2CoOOH + MnOOH + e^- \quad (2)$$

$$MnOOH + OH^- \leftrightarrow MnO_2 + H_2O + e^- \quad (3)$$

$$CoOOH + OH^- \leftrightarrow CoO_2 + H_2O + e^- \quad (4)$$

In the CV curve of GMC, redox peaks were shifted more positively upon graphene addition. Increase in potential window is a sign of increase in energy density of the material, $E = 1/2CV^2$. Such, phenomena of increase in potential window by graphene incorporation has not been reported earlier. CV curve of GMC completely engulfs the CV curve of MC which indicates the increase in area under the curve and in turn enhancement in specific capacitance of the electrode. In the CV curve of GMC, there is a noticeable increase in the electric double layer region of the curve, which suggests that apart from improving the electrical conductivity of the composite graphene also participates in the electrochemical reaction and contributes to the total capacitance.

To determine the power characteristics of the material, sweeping rate was varied and their respective voltammograms were recorded. As shown in figure 9 (a) and (b), current density increases linearly with the increase in scan rate. Even at high scan rates no distinguishable change in shape of the CV curve was observed indicating the high power capabilities of the electrode material. Superior ultrafast charge transfer in the composite material can be attributed to the unique 1D/2D hybrid nanostructure of $MnCo_2O_4$-graphene composite. Potential difference between anodic and cathodic peak of GMC is comparatively lower than MC suggesting the better capacitive performance. With the increase in scan rate anodic peaks shifts towards right and cathodic peak shift towards left. Peak shifts were caused by strengthened electric polarization and irreversible reactions at higher scan rates.

RSC Advances Accepted Manuscript

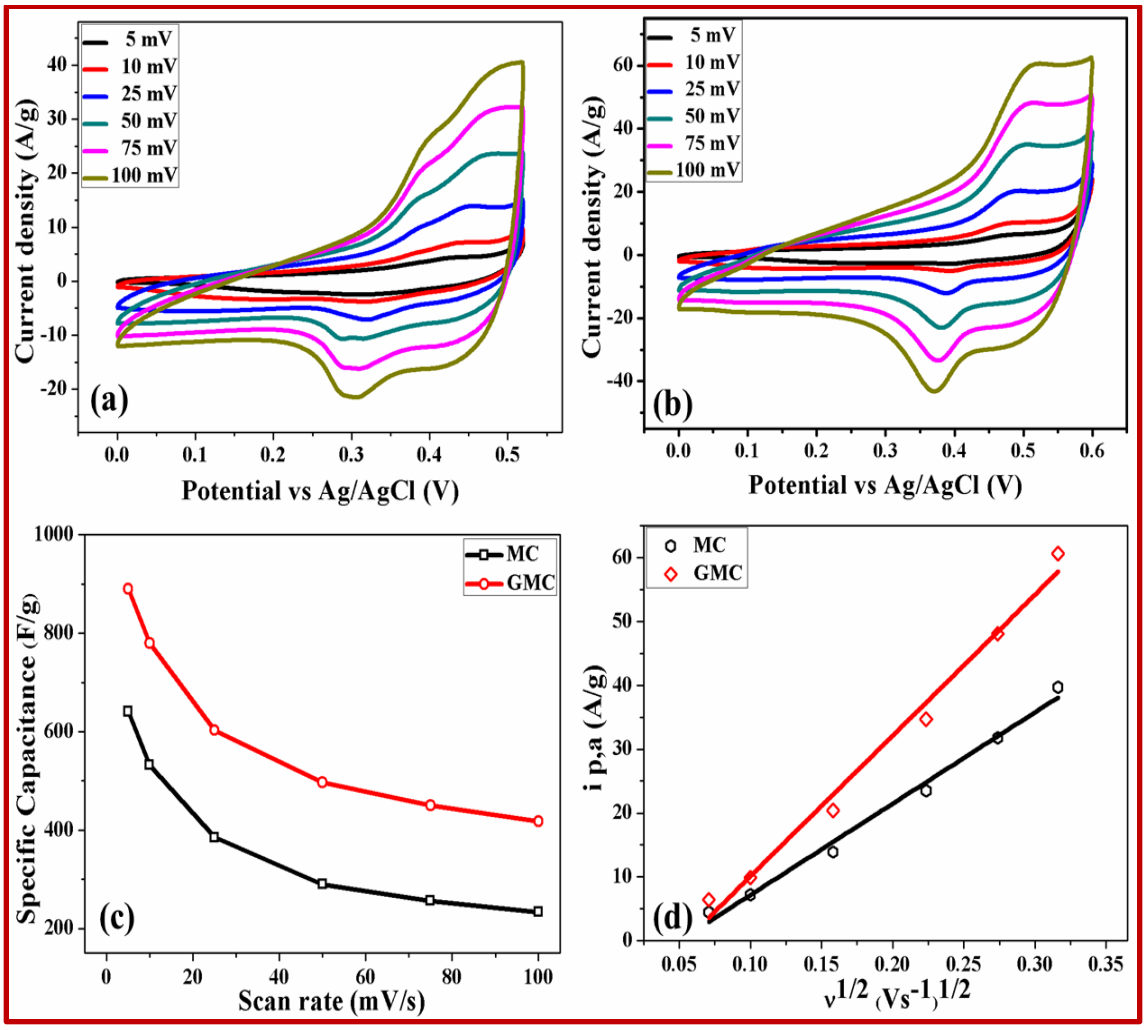

Figure 9. (a) and (b) presents the CV curve recorded at various scan rates (5 – 100 mVs^{-1}) for MC and GMC electrodes respectively, (c) graphical representation of specific capacitance calculated for different scan rates and (d) shows the Randles Sevcik plot plotted for the samples.

Compared to MC, composite material exhibits lesser shift which indicates a very high electrical reactivity and fast activation owing to high electrical conductivity. Specific capacitance (SC) of the electrodes was calculated from the CV study using below equation [36]

$$SC = \frac{1}{\nu \times m\,(V_a - V_c)} \int_{V_a}^{V_c} IV\,dV \qquad (5)$$

RSC Advances Accepted Manuscript

The SC values were calculated graphically by integrating the area under the I-V curves and then dividing by the sweep rate ν ($V\ s^{-1}$), the mass of the material (m), and the potential window (Va to Vc). As expected, GMC exhibited higher specific capacitance of 890 Fg^{-1} at 5 mV/s scan rate. While bare MC shows only 640 Fg^{-1} at the same scan rate. This remarkable enhancement can be attributed to the unique combination of 1-D/2-D hybrid nanostructure of GMC and excellent electrical conductivity of graphene that acts as an electron transport speedway. Obtained SC is superior to porous $MnCo_2O_{4.5}$ hierarchical architecture prepared by Li et al. that exhibited 151.2 F/g at 5 mV/s in KOH electrolyte [34], mesoporous $MnCo_2O_4$ spinel oxide nanostructure which demonstrates a maximum SC of 349 F/g at 5 mV/s [7], hydrothermally synthesized $MnCo_2O_4$@RGO nanocomposite prepared by Yuan et al. [6], one-dimensional $MnCo_2O_4$ nanowire arrays [41] with a specific capacitance of 349.8 F/g at the current density of 1 A/g and Co-Mn oxide/carbon-nanofiber composite electrodes with a specific capacitance of 630 F/g at the scan rate of 5 mV/s [42]. Specific capacitance calculated for other scan rates were represented graphically in figure 9 (c). At higher scan rates capacitance decreases because at low scan rate electrolyte ions will have sufficient time to diffuse into the material and avail the active species present within the bulk of the material, while at high scan rate only surface species participate in the redox process. GMC was able to retain 60 % of its actual capacitance when the scan rate was increased 20 folds while only 36 % of the capacitance was retained by bare MC. Figure 9 (d) shows the Randles Sevcik plot (anodic current density vs square root of scan rate) plotted for the samples. Straight line reveals the diffusion controlled rate kinetics of the redox process. That is electrolyte diffusion rate couldn't cope up with the rapid redox transitions occurring at electrode. Decrease in capacitance at high scan rates can also be attributed to the electrolyte ions diffusion rate controlled kinetics.

RSC Advances Accepted Manuscript

3.6.2 Chronopotentiometry (CP) Technique

Galvanostatic charge-discharge measurements were conducted for the electrode materials from 1 A/g to 10 A/g current densities. Figure 10 (a) shows the charge-discharge curve recorded at 1 A/g. Two kinds of region were noticed in the CP curves (i) linear response portion observed between 0 – 0.28 V corresponds to the electric double layer region and (ii) potential dependent current response thereafter corresponds to the faradaic redox process. An increase in the potential window for GMC was also noticed in the CP curve. Obtained results corroborate well with the CV results. Nearly symmetrical charge-discharge curves demonstrate the high reversibility of the ion transitions during oxidation and reduction. Unique combination of 1-D $MnCo_2O_{4.5}$ nanowires and 2-D graphene nanosheets has led to a remarkable increase in the charge storage ability of the material. Schematic illustrating the charge-discharge process in the composite materials is provided.

Scheme 1: Graphical representation of charging and discharging in composite electrode material.

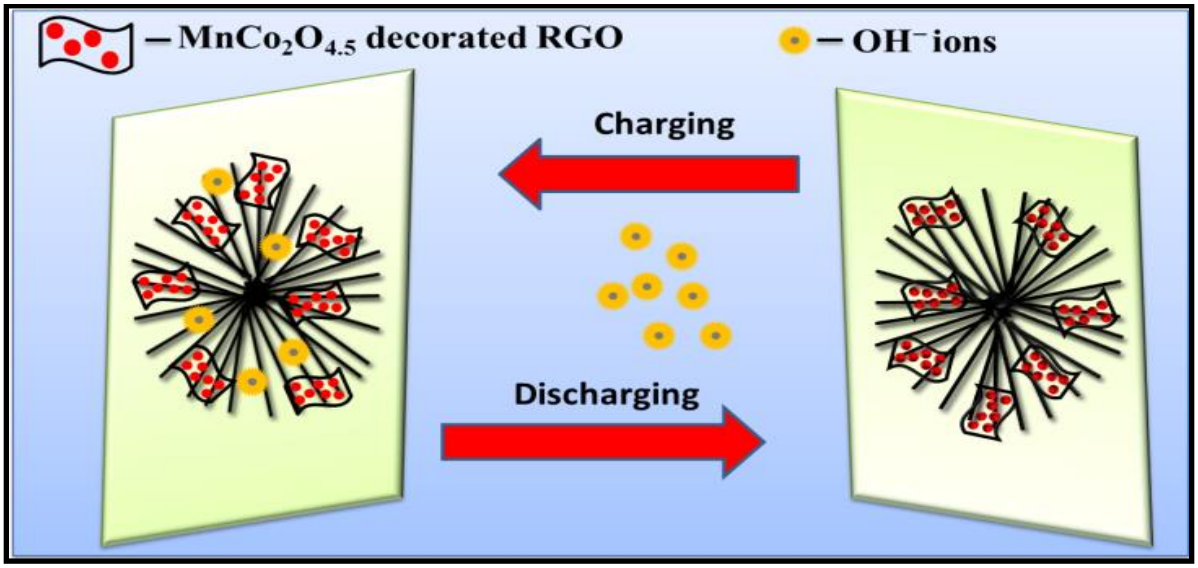

RSC Advances Accepted Manuscript

CP curves recorded at higher current densities for MC and GMC samples are presented in figure 10 (b) and 10 (c). An average columbic efficiency of 85% was exhibited by GMC against 80% shown by bare MC. Rapid ion and electron charge transport facilitated by GMC has resulted in good reversibility and higher columbic efficiency. Figure 10 (d) shows the results of continuous charging and discharging conducted for 2000 cycles to test the material's ability for long term usage.

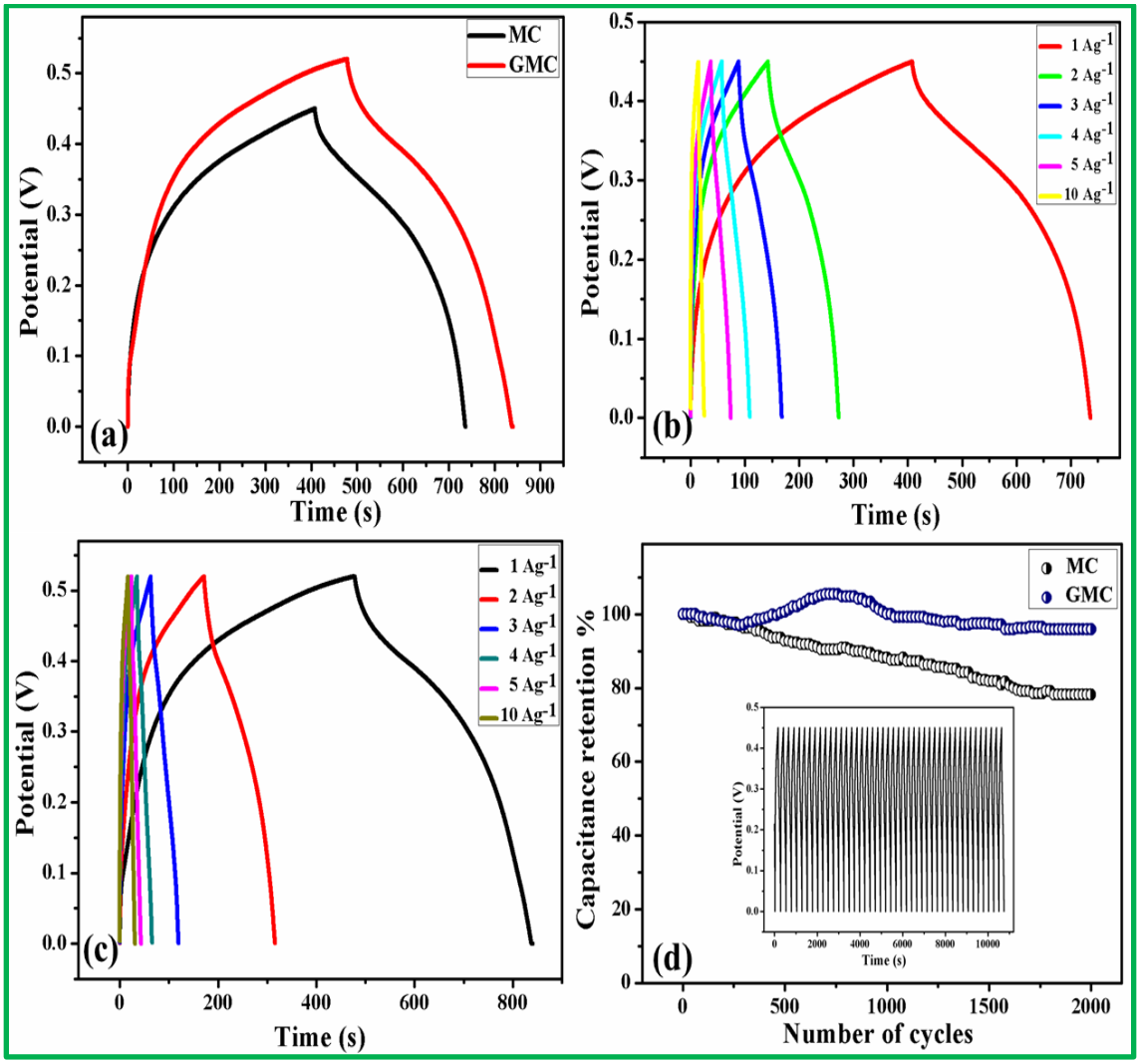

Figure 10. (a) charge-discharge curve recorded for MC and GMC at 1 A/g current density, (b) and (c) shows the CP curves of MC and GMC recorded for different (1 A/g - 10 A/g) current

RSC Advances Accepted Manuscript

densities respectively and (d) displays the cycling stability of the electrode materials conducted for 2000 continuous cycles.

Capacitance of GMC increases gradually during the initial cycles which resemble the activation process. After the activation process the material exhibited a maximum specific capacitance of 934 Fg^{-1}. Due to prolonged immersion of the electrode material in the electrolyte, ions have surplus time to diffuse into the material and access the interior reactive sites. 95% of the original capacitance was retained by GMC at the end of 2000 cycles. Whereas only 86% of the capacitance was retained by MC. This decrease can be reasoned by considering the tendency of Mn^{2+} ion dissolution in alkaline electrolytes. In the case of GMC, graphene has laminated the $MnCo_2O_{4.5}$ nanowires and prevented the degradation of Mn ions into the electrolyte. Post cycling analysis was performed to determine the structure stability of the electrode materials after continuous charging and discharging. Figure S5 in ESI provides the SEM images of the electrode materials scraped from the current collector after long charge-discharge process. Figure S5 (a) shows the distorted flower like nanowire architecture of MC. After the cycling process nanowires were found interlaced randomly. On the other hand SEM images of GMC retain the flower like structure even after the long cycling process, as shown in Figure S5 (b-d). High magnification images projects the presence of nanowire components that form the flower like architecture.

3.6.3 Electrochemical impedance spectroscopy (EIS)

In order to further reveal the transport kinetics for the electrochemical properties of $MnCo_2O_{4.5}$ samples, alternating current (AC) impedance measurements were carried between 1 Hz to 100 kHz frequency. Figure 11 displays the Nyquist plot obtained for the electrode materials. Inset of the figure shows the magnified portion of the high frequency region. Intercept

RSC Advances Accepted Manuscript

of the impedance curve at X-axis gives the measure of equivalent series resistance (ESR) or solution resistance (Rs) [41]. 2.87 Ω of ESR measured for MC decreases to 1.21 Ω with the introduction of graphene in GMC. This value is a cumulative resistance contributed by intrinsic resistance of the electrode, contact resistance between electrode and current collector and bulk electrolyte solution resistance. Semi-circle observed in the high frequency is a visual indication of charge transfer resistance (R_{ct}) originating from the discontinuity in the charge transfer at solid oxide/liquid electrolyte interface and faradaic process. Diameter of the semicircle gives an estimation of the R_{ct}. A small incomplete semicircle in the curve suggests the low charge transfer resistance of the electrode material. Slope of the line at the low frequency region represents the diffusion resistance or Warburg impedance [36].

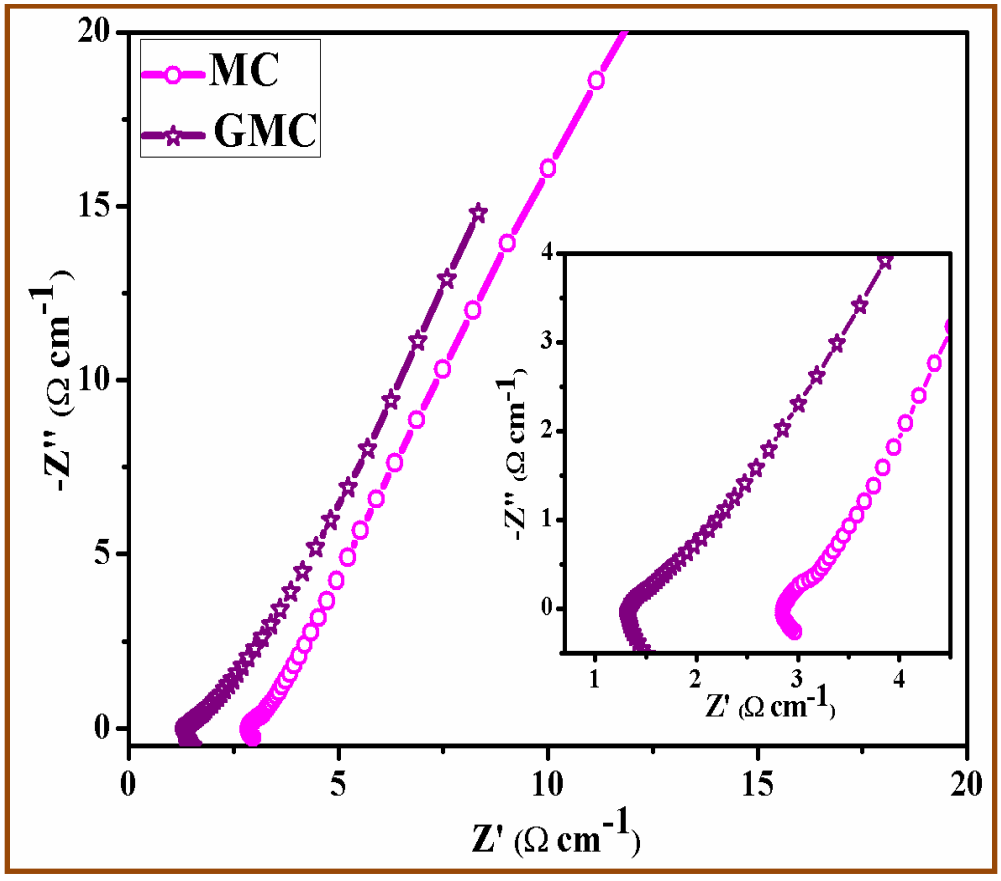

RSC Advances Accepted Manuscript

Figure 11. Shows the complex impedance plot or Nyquist plot recorded between 1 Hz – 100 kHz for the prepared samples, inset of the figures projects the magnified portion of the high frequency region.

Higher slope value of GMC indicates the rapid ion transport within the pores of the electrode material. Graphene sheets in the composite facilitate facile ion insertion/exertion in the composite material.

3.6.4 Symmetric two electrode cell assembly and electrochemical characterization

To test the real time application of the prepared GMC electrode material, a two electrode cell assembly was fabricated by a method reported earlier [43]. The symmetrical capacitor fabricated was subjected to electrochemical characterizations and the results were presented in the figure 12. CV curves recorded for three different potential windows for the symmetric capacitor using aqueous KOH electrolyte at 100 mV/s scan rate is shown in Fig. 12 (a). Operating potential window of the symmetrical cell can be extended up to 1 V. Beyond this potential, a steep current increase was noticed in the highest-voltage range, which is related to the dioxygen evolution at the electrodes [44]. Among the potential windows, 0 to 0.8 V has the highest columbic efficiency. Henceforth, all the characterizations were performed at this potential window. Faradaic behaviour of the electrode material is understood from the sloped shape of the CV curve deviating from the ideal rectangular shape observed for EDLC. Figure 12 (b) displays the CV curves recorded from low to high scan rates. Current density tends to increase with increase in scan rate depicting the high power capability of the electrode material. Specific capacitance (C_{SC}) of the cell was calculated using the below equation [44]

$$C_{SC} = \frac{4*C}{m} \qquad (6)$$

RSC Advances Accepted Manuscript

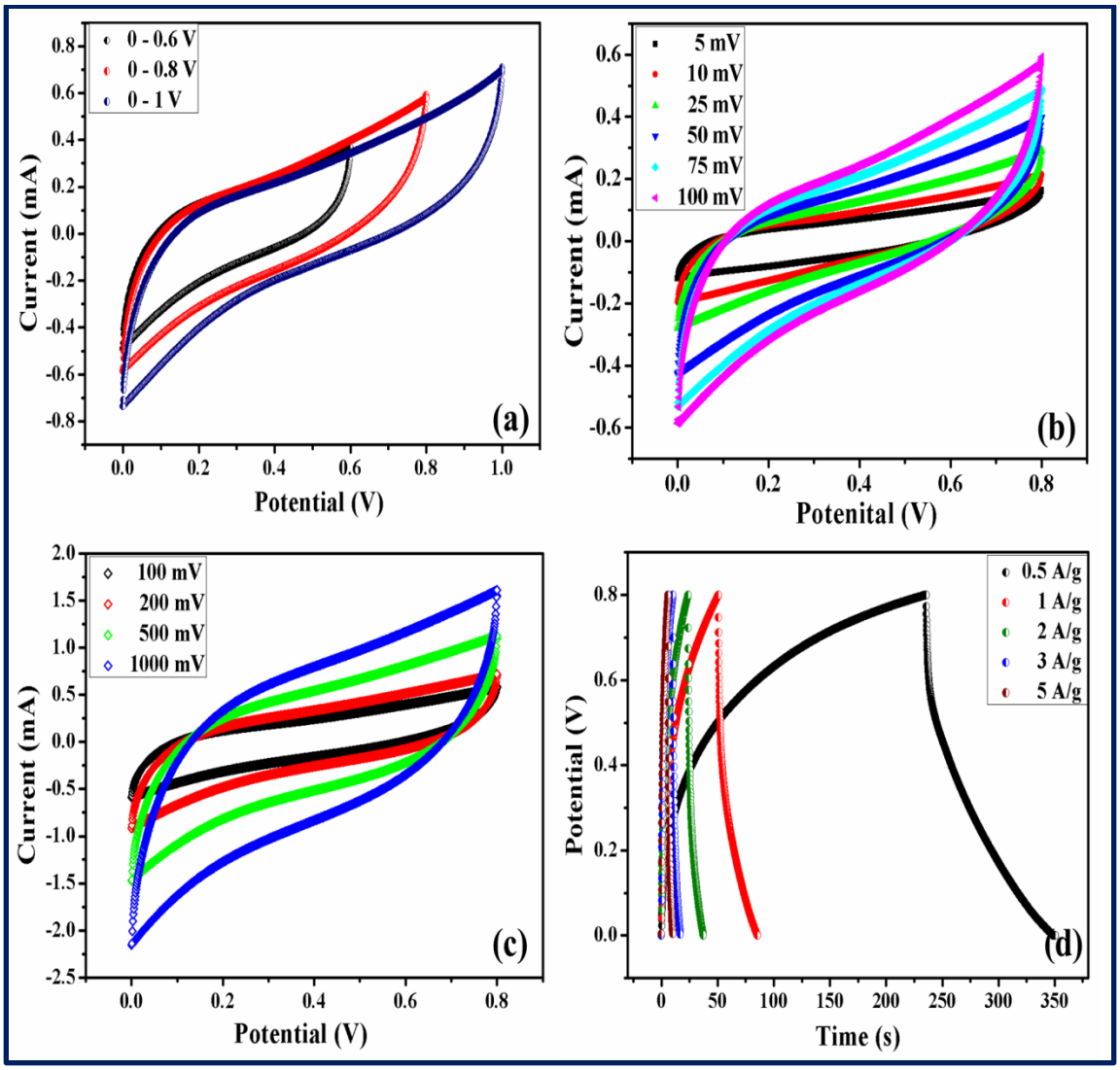

Figure 12 (a) CV curve of the symmetrical cell at three different potential windows, (b) CV curve of the cell swept at different scan rates, (c) CV curves recorded at very high scan rates and (d) Charge-discharge profile of the cell at different current densities

C- capacitance of the cell experimentally calculated, m- total mass of the electrodes. GMC exhibits a specific capacitance of 189 Fg^{-1} at 5 mV/s scan rate. Figure 12 (c) demonstrates the ultrafast electrochemical reactivity of the electrode material at very high scan rates. Linear increase in current density with negligible change in the CV shape depicts the high rate

RSC Advances Accepted Manuscript

performance of the as prepared hybrid electrode material. This ultrafast charge transport can be attributed the excellent electrical support provided by graphene in the composite. Further, charge-discharge curves recorded at different current densities is shown in Fig. 12 (d). Rate kinetics of the cell was analyzed using electrochemical impedance spectroscopy which reveals the low resistive characteristics of the material (Fig. 13 (a)). A low ESR value of 1.43 Ω was observed for the cell. Inset of the Fig. 13 (a) shows the magnified portion of the high frequency region. Near absence of semicircle in this region indicates the negligible charge transfer resistance of the electrode material. This once again confirms the tendency of graphene to act as electron transport highway. Straight line observed in the low frequency region suggests the lower diffusion resistance or Warburg impedance offered by the material. Figure 13 (b) presents the rangone plot plotted for the GMC based symmetrical cell. This illustrates the ideal balance between the energy density and the power density.

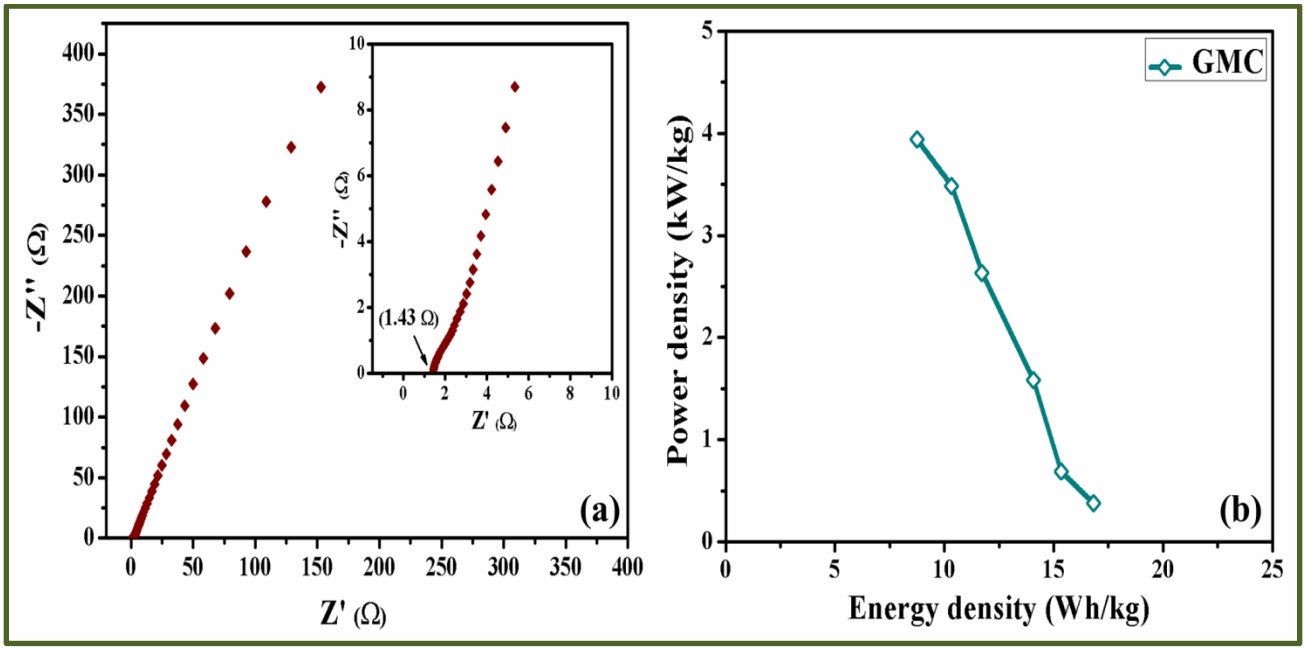

Figure 13 (a) Nyquist plot obtained from AC impedance measurements (inset shows magnified portion of high frequency region) and (b) Rangone plot plotted for the symmetric cell

RSC Advances Accepted Manuscript

4. Conclusions

Distinct 1-D/2-D hybrid nanostructured manganese cobaltite-graphene nanocomposite was synthesized by facile hydrothermal method. Successful compound formation was determined from XRD structural study, FTIR and XPS chemical analyses. Flower like architecture formed by clusters of $MnCo_2O_{4.5}$ nanowires was observed for MC. By graphene incorporation a unique hybrid 1-D/2-D nanostructure was developed in the composite material. Exceptionally high BET surface area measured for the composite testifies the superiority of the hybrid nanostructure. CV measurements reveal the excellent redox reactivity of the prepared electrode materials. GMC exhibited a high specific capacitance of 890 F/g which upon activation over cycling increases to 934 F/g. $MnCo_2O_{4.5}$ decorated graphene sheets in the composite provides high interfacial sites for the redox process, exceptional electrical support and mechanical strength during cycling. The manganese cobaltite-graphene composite was able to retain 95% of its original capacitance at the end of 2000 cycles. The small solution resistance value of 1.21 Ω demonstrates the superior conductivity of the composite material. A symmetrical cell fabricated using GMC electrode material exhibited a maximum specific capacitance of 189 F/g at 5 mV/s scan rate. Ultrafast charge transfer and accelerated rate kinetics owing to graphene incorporation was understood from the CV curves recorded at high scan rates and Nyquist plot. Superior performance of the hybrid composite makes it a potential candidate for supercapacitor applications.

ACKNOWLEDGMENT

RSC Advances Accepted Manuscript

Financial support from Anna University by providing Anna Centenary Research Fellowship (ACRF) for one of the author A. Nirmalesh Naveen was greatly appreciated (Lr.No.CR/ACRF/2013/37)

REFERENCES

1. Wang, L.; Wang, X.; Xiao, X.; Xu, F.; Sun, Y.; Li, Z. Reduced graphene oxide/nickel cobaltite nanoflake composites for high specific capacitance supercapacitors. Electrochimica Acta **2013**, 111, 937– 945.
2. Su, X.; Yu, L.; Cheng, G.; Zhang, H.; Sun, M.; Zhang, X. High-performance a-MnO2 nanowire electrode for supercapacitors. (In Press, Corrected Proof), Doi:10.1016/j.apenergy.2014.07.094.
3. Han, D.; Xu, P.; Jing, X.; Wang, J.; Song, D.; Liu, J.; Zhang, M. Facile approach to prepare hollow core–shell NiO microspherers for supercapacitor electrodes. Journal of Solid State Chemistry **2013**, 203, 60–67.
4. Zhi, J.; Deng, S.; Zhang, Y.; Wang, Y.; Hu, A. Embedding Co3O4 nanoparticles in SBA-15 supported carbon nanomembrane for advanced supercapacitor materials. J. Mater. Chem. A **2013**, 1, 3171-3176.
5. Zhao D.; Xu, M.W.; Zhou, W.J.; Zhang, J.; Li, H.L. Preparation of ordered mesoporous nickel oxide film electrodes via lyotropic liquid crystal templated electrodeposition route. Electrochimica Acta **2008**, 53, 2699–2705.
6. Yuan Y.; Bi H.; He G.; Zhu, J.; Chen H. A Facile Hydrothermal Synthesis of a $MnCo_2O_4$@Reduced Graphene Oxide Nanocomposite for Application in Supercapacitors. Chem. Lett. **2014**, 43, 83–85.

RSC Advances Accepted Manuscript

7. Padmanathan, N.; Selladurai, S. Mesoporous MnCo2O4 spinel oxide nanostructure synthesized by solvothermal technique for supercapacitor. Ionics **2014,** 20, 479–487.
8. Yang, Q.; Lu, Z.; Chang, Z.; Zhu, W.; Sun, J.; Liu, J.; Sun, X.; Duan, X. Hierarchical Co3O4 nanosheet@nanowire arrays with enhanced pseudocapacitive performance. RSC Adv., **2012**, 2, 1663-1668.
9. Zhang, J.; Shu, D.; Zhang, T.; Chen, H.; Zhao, H.; Wang, Y.; Sun, Z.; Tang, S.; Fang, X.; Cao, X. Capacitive properties of PANI/MnO2 synthesized via simultaneous-oxidation route. Journal of Alloys and Compounds **2012,** 532, 1– 9.
10. Chen, Y.C.; Hsu, Y.K.; Lin, Y.G.; Lin, Y.K.; Horng, Y.Y.; Chen, L.C.; Chen, K.H. Highly flexible supercapacitors with manganese oxide nanosheet/carbon cloth electrode. Electrochimica Acta **2011**, 56, 7124– 7130.
11. Yoon, Y.L.; Ko, J.M. CoNi Oxide/Carbon-Nanofiber Composite Electrodes for Supercapacitors. Int. J. Electrochem. Sci. **2008,** 3, 1340 – 1347.
12. Luo, J.M.; Gao, B.; Zhang, X.G. High capacitive performance of nanostructured Mn–Ni–Co oxide composites for supercapacitor. Materials Research Bulletin **2008,** 43, 1119–1125.
13. Hu, L.; Zhong, H.; Zheng, X.; Huang, Y.; Zhang, P.; Chen, Q. CoMn2O4 Spinel Hierarchical Microspheres Assembled with Porous Nanosheets as Stable Anodes for Lithium-ion Batteries. SCIENTIFIC REPORTS **2012**, 2:986, 1-8.
14. Naveen, A.N.; Selladurai, S. Novel synthesis of highly porous spinel cobaltite (NiCo2O4) electrode material for supercapacitor applications. AIP Conference Proceedings **2014**, 1591, 246-248.

RSC Advances Accepted Manuscript

15. Jiang, S.; Shi, T.; Long, H.; Sun, Y.; Zhou, W.; Tang, Z. High-performance binder-free supercapacitor electrode by direct growth of cobalt-manganese composite oxide nansostructures on nickel foam. Nanoscale Research Letters **2014**, 9:492, 1-8.
16. Xu, Y.; Wang, X.; An, C.; Wang, Y.; Jiao, L.; Yuan, H. Facile synthesis route of porous MnCo2O4 and CoMn2O4 nanowires and their excellent electrochemical properties in supercapacitor. J. Mater. Chem. A, **2014**, 2, 16480-16488.
17. Shaijumon, M.M. Ou, F.S.; Ci, L.; Ajayan, P.M. Synthesis of hybrid nanowire arrays and their application as high power supercapacitor electrodes. Chem. Commun., **2008**, 2373-2375.
18. Wang, X.; Wang, X.; Huang, W.; Sebastian, P.J.; Gamboa, S. Sol–gel template synthesis of highly ordered MnO2 nanowire arrays. Journal of Power Sources **2005,** 140, 211–215.
19. Xia X.H.,; Tu, J.P.; Mai, Y.J.; Wang, X.L.; Gu, C.D.; Zhao, X.B. Self-supported hydrothermal synthesized hollow Co3O4 nanowire arrays with high supercapacitor capacitance. J. Mater. Chem., **2011**, 21, 9319–9325.
20. Li, L.; He, F; Gai, S.; Zhang, S.; Gao, P.; Zhang, M.; Chen, Y.; Yang, P. Hollow structured and flower-like C@MnCo2O4 composite for high electrochemical performance in a supercapacitor, CrystEngComm. **2014**, 16, 9873 –9881.
21. Lv, W.; Sun, F.; Tang, D.M.; Fang, H.T.; Liu, C.; Yang, Q.H.; Cheng, H.M. A sandwich structure of graphene and nickel oxide with excellent supercapacitive performance. J. Mater. Chem., **2011**, 21, 9014–9019.
22. Ren, L.; Hui, K.S.; Hui, K.N. Self-assembled free-standing three-dimensional nickel nanoparticle/graphene aerogel for direct ethanol fuel cells. J. Mater. Chem. A, **2013**, 1, 5689–5694.

RSC Advances Accepted Manuscript

23. Mishra, A.K.; Ramaprabhu, S. Functionalized Graphene-Based Nanocomposites for Supercapacitor Application. J. Phys. Chem. C **2011**, 115, 14006–14013.
24. Ji, Z.; Zhu, G.; Shen, X.; Zhou, H.; Wu, C.; Wang, M. Reduced graphene oxide supported FePt alloy nanoparticles with high electrocatalytic performance for methanol oxidation. New J. Chem., **2012**, 36, 1774–1780.
25. Kaniyoor, A.; Baby, T.T.; Ramaprabhu, S. Graphene synthesis via hydrogen induced low temperature exfoliation of graphite oxide. J. Mater. Chem., **2010**, 20, 8467–8469.
26. Yang, W.; Hao, J.; Zhang, Z.; Lu, B.; Zhang, B.; Tang, J. Synthesis of hierarchical MnCo2O4.5 nanostructure modified MnOOH nanorods for catalytic degradation of methylene blue. Catalysis Communications **2014**, 46, 174–178.
27. Naveen, A.N.; Selladurai, S. Tailoring structural, optical and magnetic properties of spinel type cobalt oxide (Co3O4) by manganese doping. Physica B 2015, 457, 251–262.
28. Xie, L.; Li, K.; Sun.; G.; Hu, Z.; Lv, C.; Wang, J.; Zhang, C. Preparation and electrochemical performance of the layered cobalt oxide (Co3O4) as supercapacitor electrode material. J Solid State Electrochem **2013,** 17, 55–61.
29. Chen, W.; Yan, L. Preparation of graphene by a low-temperature thermal reduction at atmosphere pressure. Nanoscale, **2010**, 2, 559–563.
30. Wang H.W., Hu, Z.A.; Chang, Y.Q.; Chen, Y.L.; Wu, H.Y.; Zhang, Z.Y.; Yang, Y.Y. Design and synthesis of NiCo2O4–reduced graphene oxide composites for high performance supercapacitors. J. Mater. Chem., **2011**, 21, 10504–10511.
31. Srivastava, M.; Uddin, M.E.; Singh, J.; Kim, N.H.; Lee, J.H. Preparation and characterization of self-assembled layer by layer NiCo2O4–reduced graphene oxide

RSC Advances Accepted Manuscript

nanocomposite with improved electrocatalytic properties. Journal of Alloys and Compounds **2014**, 590, 266–276.

32. Fang, D.L.; Wu, B.C.; Yan, Y.; Mao, A.Q.; Zheng, C.H. Synthesis and characterization of mesoporous Mn–Ni oxides for supercapacitors. J Solid State Electrochem **2012,** 16, 135–142.
33. Mondal, A.K.; Su, D.; Chen,S.; Ung, A.; Kim, H.S.; Wang, G. Mesoporous MnCo2O4 with a Flake-Like Structure as Advanced Electrode Materials for Lithium-Ion Batteries and Supercapacitors. Chem. Eur. J. **2015**, 21, 1526 – 1532.
34. Li, W.; Xu, K.; Song, G.; Zhou, X.; Zou, R.; Yang, J.; Chen, Z; Hu, J. Facile synthesis of porous MnCo2O4.5 hierarchical architectures for high-rate supercapacitors. CrystEngComm, **2014**, 16, 2335–2339.
35. Li, J.; Wang, J.; Liang, X.; Zhang, Z.; Liu, H. Qian, Y.; Xiong, S. Hollow MnCo2O4 Submicrospheres with Multilevel Interiors: From Mesoporous Spheres to Yolk-in-Double-Shell Structures. ACS Appl. Mater. Interfaces **2014**, 6, 24−30.
36. Naveen, A.N.; Selladurai, S. Investigation on physiochemical properties of Mn substituted spinel cobalt oxide for supercapacitor applications. Electrochimica Acta **2014,** 125, 404–414.
37. Toupin, M.; Brousse, T.; Be´langer, D. Charge Storage Mechanism of MnO2 Electrode Used in Aqueous Electrochemical Capacitor. Chem. Mater. **2004**, 16, 3184-3190.
38. Yang, D.; Velamakanni, A.; Bozoklu, G.; Park, S.; Stoller, M.; Piner, R.D.; Stankovich, S.; Jung, I.; Field, D.A.,; Ventrice Jr,C.A.; Ruoff, R.S. Chemical analysis of graphene oxide films after heat and chemical treatments by X-ray photoelectron and Micro-Raman spectroscopy. CARBON **2009**, 47, 145–152.

RSC Advances Accepted Manuscript

39. Vijayakumar, S.; Nagamuthu, S.; Muralidharan G. Supercapacitor Studies on NiO Nanoflakes Synthesized Through a Microwave Route. ACS Appl. Mater. Interfaces **2013**, 5, 2188−2196.

40. Li, L.; Zhang, Y.; Shi, F.; Zhang, Y.; Zhang, J.; Gu, C.; Wang, X.; Tu, J. Spinel Manganese−Nickel−Cobalt Ternary Oxide Nanowire Array for High-Performance Electrochemical Capacitor Applications. ACS Appl. Mater. Interfaces **2014**, 6, 18040−18047.

41. Li, L.; Zhang, Y.Q.; Liu, X.Y.; Shi, S.J.; Zhao, X.Y.; Zhang, H.; Ge, X.; Cai, G.F.; Gu, C.D.; Wang, X.L.; Tu, J.P. One-dimension MnCo2O4 nanowire arrays for electrochemical energy storage. Electrochimica Acta **2014**, 116, 467– 474.

42. Kim, S.H.; Kim, Y.I.; Park, J.H.; Ko, J.M. Cobalt-Manganese Oxide/Carbon-nanofiber Composite Electrodes for Supercapacitors. Int. J. Electrochem. Sci. **2009**, 4, 1489 – 1496.

43. Naveen, A.N.; Selladurai, S. Novel low temperature synthesis and electrochemical characterization of mesoporous nickel cobaltite-reduced graphene oxide (RGO) composite for supercapacitor application. Electrochimica Acta **2015**, 173, 290–301.

44. Khomenko, V.; Raymundo-Pinero, E.; Frackowiak, E.; Béguin, F. High-voltage asymmetric supercapacitors operating in aqueous electrolyte, Appl. Phys. A **2006**, 82, 567–573.

45. Bello, A.; Fashedemi, O. O.; Lekitima, J.N.; Fabiane, M.; Dodoo-Arhin, D.; Ozoemena, K.I.; Gogotsi, Y.; Charlie Johnson, A.T.; Manyala, N. High-performance symmetric electrochemical capacitor based on graphene foam and nanostructured manganese oxide, AIP ADVANCES **2013**, 3, 082118(1-9).

RSC Advances Accepted Manuscript

Graphical Abstract

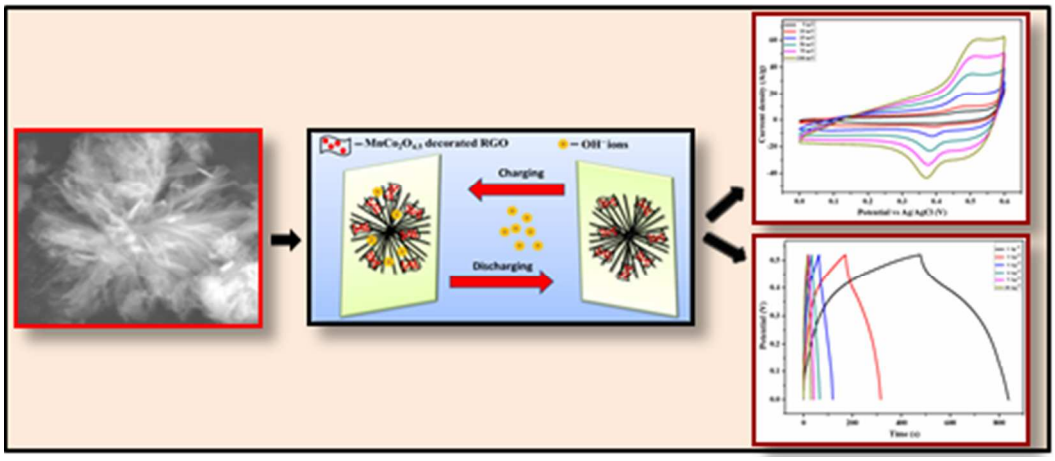

Textual Abstract

- A novel method to bridge the advantages of 1D and 2D nanomaterials for energy storage application

RSC Advances Accepted Manuscript